IEEE Access
Multidisciplinary ⋮ Rapid Review ⋮ Open Access Journal

Received August 6, 2019, accepted August 13, 2019, date of publication August 30, 2019, date of current version October 22, 2019.

Digital Object Identifier 10.1109/ACCESS.2019.2937137

SID: Sensor-Assisted Image Deblurring System for Mobile Devices

QING WANG, JUN TAN, TIANZHANG XING, FENG CHEN, AND JINPING NIU
Shaanxi International Joint Research Centre for the Internet of Things, School of Information Science and Technology, Northwest University, Xi'an, China

Corresponding author: Tianzhang Xing (xtz@nwu.edu.cn)

This work was supported in part by the Project NSFC under Grant 61602381, Grant 61501372, and Grant 61602382, in part by the China Postdoctoral Science Foundation under Grant 2017M613187 and Grant 2017M613186, and in part by the Natural Science Basis Research Plan in Shaanxi Province of China under Grant 2017JM6074.

ABSTRACT Handheld mobile photography is often affected by motion blur due to the difficulty of keeping the camera's stable. The existing processing method is usually a high-cost deblurring process of a computer, which seriously affects the user experience, and the deblurring effect is poor due to the lack of information on camera motion. Inspire by edging computing's ongoing efforts in automatically and collaboratively process more types of resources in the edge and cloud. In this paper, we present SID, a sensor-assisted image deblurring system for mobile devices. Using information about camera motion acquired from built-in sensors from smartphones (e.g. accelerometers, gyroscopes, and magnetometers), then estimating the point spread function, and combining the image's segmentation smoothing characteristics with spatial adaptation to image Deblurring. The image is preprocessed by the p-m nonlinear diffusion model, which preserves the characteristics of the image. The fuzzy image confirmation avoids the damage to the original high quality image. Wiener-Hoff optimization is used to optimize the effect of image restoration. We evaluated 400 photos with varying degrees of blur and size. Compared to traditional blind and unblind deconvolution methods, our algorithm shows significant advantages in both deblurring and processing delays.

INDEX TERMS Mobile computing, motion blur, sensor, image processing.

I. INTRODUCTION

With the rapid development of social networks, smart terminals and mobile internet technologies, mobile photography has gradually changed people's social lifestyles, and has become an indispensable part of people's daily lives [7]–[9]. People have higher requirements for the function of the camera and the quality of the pictures, they even hope cameras to be 'smart' like people. For example, cameras can automatically classify and manage images [31], [36], fix blurred images, clean up useless images, etc. These smart technologies are attracting more and more attention from academia and industry. In real life, most users find it difficult to keep the camera of the phone stable during shooting (for example, the user is in a moving vehicle environment or shooting a moving target), so that the captured photos usually have different degrees of [2] or virtual focus blur [15]. In this paper, we focus on image deblurring techniques which are very important in many applications, It helps to improve the quality of the image, thus improving the accuracy of image recognition. High-quality images help identify and resolve physical objects. For example, face recognition [12] can verify user identity, control service access, and establish trust in objects and cloud services, and the map software can locate the user's geographic location through street view recognition, thereby providing users with location-related services [25], [26], [28], [40]. In addition, image recognition also commonly used as a ground truth for wireless signal counting crowds [35]. These applications all have requirements for image quality, so it is necessary to study image deblurring techniques to improve image quality, in which image motion deblurring is a hot topic in recent years, However, if there is no information about camera motion, it is still a difficult problem to remove blur from general smartphone photos.

At present, mainstream images restoration algorithms, such as linear algebraic reconstruction algorithms, are based on the statistical properties of known noise and qualitative operators [15]. These methods need to solve the point spread function and evaluate the environmental noise in

The associate editor coordinating the review of this article and approving it for publication was Honghao Gao.

advance. In addition, the inverse filtering algorithm is another commonly used image restoration algorithm, and its computational overhead is as large as the linear algebra reconstruction algorithm because they to process the entire image [5]. Therefore, if the above image restoration methods are used on a mobile terminal, we will encounter the following two challenges:

- Point spread function missing: Classical algorithms need to predict point spread functions, but in practice, parameter characteristics are unpredictable and cannot be calculated. Therefore, the missing point diffusion function is an unavoidable problem of mobile devices to complete the picture deblurring.
- Large computational overhead: Most existing deblurring algorithms uses iterative and recursive computational methods, the computational overhead are large. When using these methods on resource-constrained mobile devices, algorithm optimization is first required to reduce computational overhead [17].

A better approach is to estimate the PSF [1] by tracking the motion of the camera and using the data from the auxiliary high-speed low-resolution camera. Today, most mobile devices are now equipped with multiple sensors (gyroscopes, accelerometers, etc.). There have been many applications based on mobile phone sensor data, such as human activity recognition [21], [39], location awareness [41], [43], anti-fall for the elderly, human health monitoring, etc. From these sensors, information about camera motion can be obtained, and fuzzy psf can be calculated. In this paper, we studied the sensor-assisted single image deblurring technique for smartphones. The main idea is to fuse the direction of the 3D camera calculated from the sensor data of the mobile device to estimate the blur psf. And combine the spatial adaptive idea of the image and the segmentation smoothing to realize the image deblurring process. Before processing, we used the p-m nonlinear diffusion model to preprocess the image to eliminate noise while preserving image features. After the denoising process, we performed a fuzzy type confirmation on the image to avoid processing the nonplussed image and destroying the original clear image. Point spread function estimation and nonlinear deblurring systems are used to deblur the graphics. Finally, we optimized the image deblurring effect. Because the camera's rotational motion is calculated from real-time sensor data, we can estimate the point spread function to deblur the blurred image. The contributions of our work are summarized as follows:

- We propose a lightweight P-M nonlinear diffusion model which can be ported to mobile devices. P-M model is very good at removing the noise of photos taken by the mobile phone, while also retaining the characteristics of the photos.
- We propose a fuzzy image confirmation algorithm which ensures the correctness of the image processed by the system, avoids processing the non-blurred image, and destroys the original high quality image.
- The SID system we designed can deblur the image without prior knowledge and can significantly reduce the cost of computing resources and can run on mobile devices.

II. PRELIMINARIES

A. BLUR PICTURE AND CAMERA MOVEMENT

Photos with different degrees of blurring may be taken due to different degrees of hand shake in the photo taking process. Figure 1 shows several photographs of different degrees of blurring taken when a person is at rest and walking due to hand shake.

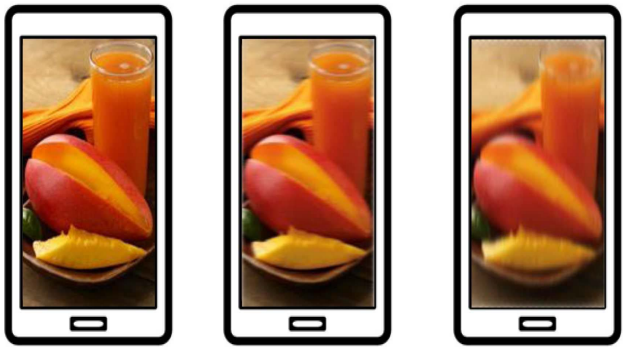

(a) Static. (b) Little shake. (c) Take in walking.

FIGURE 1. Different degrees of fuzzy photos when the hand is static, slight shake, and taking picture in walking.

If the entire image is used as input to the deblurring system, the estimate of the point spread function is very expensive. Many existing studies have shown that knowledge of the form of camera motion models can be used to solve complex spatial variability problems. The blurred image can be presented as the integral of all intermediate images captured by the camera along the motion trajectory [37], [42]. The motion of the camera can be simulated with the camera's three-dimensional motion or 6d camera motion, with in-plane translation and rotation [10]. In order to speed up the optimization, a fast patch-based non-uniform deblurring method has been proposed [11]. These prior knowledge has been proved to be helpful.

Inertial sensors such as gyroscopes and accelerometers can be utilized to obtain more accurate camera motion information. These sensors have been incorporated into many common mobile devices. Reference [30] proposed a smart phone deblurring system based on gyroscope readings to synthesize local fuzzy Kernels. Compared with the existing deblurring algorithm, the system has a good effect. But user interaction is needed to synchronize the camera and gyro sensor. Josh *et al.* [14] established a well-designed DSLR-based camera system that assumes that the inertial sensors are pre-calibrated and synchronized. However, due to the drift problem of noise sensor reading, single sensor data can not achieve effective image deblurring. This paper combines multi-sensor data information to calculate the camera's

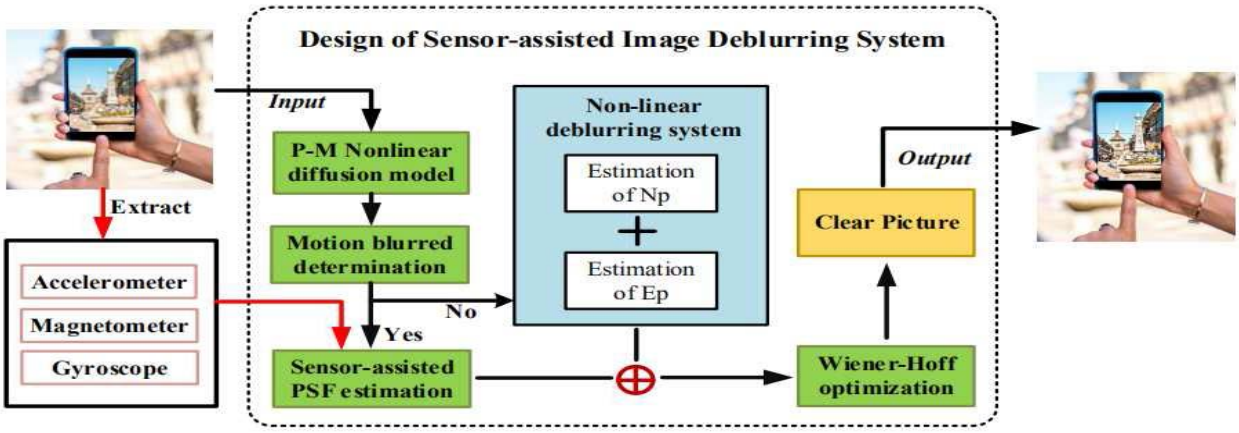

FIGURE 2. The overview of system.

motion direction. Camera motion includes translation and rotation. In this work, we only consider the rotational motion of the camera, because the motion blur is mainly caused by the rotation of the camera. Secondly, the camera translation estimation based on acceleration is prone to error, and the acceleration data needs to be integrated twice to get the panning of the camera, the effect of camera panning can be ignored in the short time interval of the photo. In our work, the sensor reading drifts, that is, the gyro drift, and the camera motion is the rotary motion. In order to more accurately estimate the camera's motion direction and reduce the gyro drift, we use an accelerometer to provide the gravity vector, and the gyroscope provides the angular rotation speed of the camera's three-axis, combined with the direction of the compass provided by the magnetometer, is used to estimate the orientation of the three-dimensional camera. For the low quality data (noise data or abnormal data) in the sensor, we can refer to the method proposed in [4] for processing.

B. WIENER FILTER

A filter is a device that filters out noise and interference from continuous or discrete input data to extract useful information. The Wiener filter commonly used in image processing is an optimal estimation based on the minimum mean square error criterion [18], which minimizes the mean square error between the input and output of the filter, and is often used for the recovery of damaged images. However, this method cannot be used for random processes where noise is unstable.

The improved Wiener filter, inverse filter, and other methods all assume that the noise caused by external factors is known, and the point spread function can be accurately estimated. However, in the real environment, such prior knowledge is difficult to obtain in advance, which limits the application of winner filtering in mobile terminals.

In this paper, we use the sensor data(e.g. accelerometer, magnetometer, and gyroscope and so on) from the mobile terminal to calculate the orientation of the camera motion, then estimate the point spread function and design a nonlinear defusing system to de-blurring the image. Finally, optimizing the de-blurring effect by the Wiener-Hoff equation. The specific details will be introduced in the section IV.

III. SYSTEM OVERVIEW

The system framework is shown in Figure 2. Images captured by the phone serve as input to the system, these pictures become blurred due to hand jitter, less vibration, or hardware noise such as cell phone photo sensor. These pictures can be processed through the following modules designed in the system to improve their quality:

P-M nonlinear diffusion model: The model is used for image denoising processing, it is the first step of system image processing, all images need to be processed by the model before motion blurred determination. which acts like user authentication in a privacy protection system [24], [27]. The advantage of the P-M nonlinear diffusion model is it can maintain the boundary of a nonlinear diffusion equation to overcome the shortcomings of linear diffusion filter, and the image denoising effect is greatly improved. In addition, the image border outline does not spread and the image texture remains clear.

Motion blurred determination: Since our system is mainly aimed at the recovery of motion blur graphics. It is necessary to judge the blurred categories of images before image deblurring, which can avoid damage to the original high quality image. The image for motion blur needs to extract the corresponding sensor data to estimate the point spread function which is used as the boundary condition of the nonlinear deblurring system to process the image. For non-motion blurred images, they are directly processed by the nonlinear deblurring system after image preprocessing. The method of judgment is in the section IV-B.

Sensor-assisted PSF estimation: We combine the data from the accelerometer, magnetometer, and gyroscope to calculate the orientation of the camera before and after the photo is captured, and then estimate the point spread function (PSF).

Non-linear deblurring system: A non-linear deblurring system is designed based on the estimated point spread function to process the blurred image, which determines the pixel area and edge pixel points of the target in the image by respectively estimating the moving pixel area and estimating the edge pixel area.

Wiener-Hoff optimization: Finally, we use the Wiener-Hoff equation to optimize our system. The deblurred picture is denoised by a median filter, so that the mean square error between the images before and after processing satisfies parameter J to achieve deblurring optimization.

IV. SYSTEM DESIGN

A. P-M NONLINEAR DIFFUSION MODEL

In recent years, nonlinear diffusion denoising method has been widely used in the field of image processing. The non-linear diffusion process is a kinetic description that conforms to the thermal diffusion process in physics. It can remove the noise while following-up work and keep the outline of the image from being diffused, and the texture in the image remains sharp. Partial differential equation [19] is a typical nonlinear diffusion denoising method.

1) MODEL DESIGN

In physics, if there is some kind of impurity in the medium (such as gas, liquid and solid), and its concentration distribution is not uniform, the impurity will migrate from the high concentration area to the low concentration area. The function u(x, y, t) represents the concentration with time and space changes, then the spatial distribution of non-uniform gradient can be used to express ∇u. Under certain conditions, the relationship between the flux and the concentration gradient is:

$$J = -D\nabla u \tag{1}$$

In (1), the negative sign indicates that the flux moves from high concentration to low concentration. D is the diffusion tensor and is a positive definite symmetric matrix. Impurities in the proliferation process will not produce new and will not be lost, so can be expressed as a continuous equation as follows:

$$\frac{\partial u}{\partial t} = -divJ \tag{2}$$

In the (2), t is time. Substituting (1) into (2) gives the diffusion equation:

$$\frac{\partial u}{\partial t} = -div(D \times \nabla u) \tag{3}$$

Applying the theory of physical diffusion to the image denoising algorithm, in order to achieve denoising and meanwhile preserving the edge. It is hoped that the conduction coefficient will increase automatically in the area where the image is flat and the smaller irregular fluctuation noise in the flat area will be Smooth, and near the edge of the image, the conduction coefficient can be automatically reduced so that the edge is almost unaffected. Therefore, Perona and Malik first proposed the following nonlinear diffusion model:

$$\begin{cases} \dfrac{\partial u_t}{\partial t} = -div[g(|\nabla u_t|)\nabla u_t] \\ u(x, y, 0) = u_0(x, y) \end{cases} \tag{4}$$

In the (4), u_t is the image at time t, and ∇u_t is the gradient of the image. The function $g(|\nabla u_t|)$ is called a diffusion function whose value represents the diffusion intensity, usually a smooth monotonously decreasing function with non-negative $g(|\nabla u_t|)$, given in two forms:

$$g(|\nabla u_t|) = \frac{1}{1 + \frac{|\nabla u_t|^2}{k}} \tag{5}$$

and

$$g(|\nabla u_t|) = e^{-(\frac{|\nabla u_t|}{k})^2} \tag{6}$$

In the (5) and (6), k is the gradient threshold. The P-M nonlinear diffusion model can suppress the contradiction between noise and edge-preserving texture and achieve better results.

B. MOTION BLURRED IMAGE DETERMINATION

In our system, we hope the image to be processed to be a motion blurred image, so we first need to make a fuzzy judgment on the image to avoid processing the non-blurred image and destroying the original clear image. There are two main steps in the determination of motion blurred images. We first determine whether the image is blurred by evaluating the sharpness of the image. Secondly, we use the frequency spectrum after the Fourier transform of the blurred image to determine the blur type of the image.

1) FUZZY IMAGE CONFIRMATION

In image processing, the sharpness of an image is usually used to determine whether the image is blurred. There are three common methods for evaluating the sharpness of an image. One is to detect the edge information of the image, this method relies on the edge detection method of the image. The second method is based on the pixel values of the image, although its computational complexity is low, but it is susceptible to noise. The third method is based on high frequency information of the image, although its performance is better than the first two methods, it requires the conversion of the image from the time domain to the frequency domain, which has high computational complexity and is not suitable for real-time systems. In order to reduce the processing delay of the system, we use the findings that gradient images of natural images have a heavy-tailed distribution and blurred images do not have such a distribution by Fergus *et al.* [6] to distinguish between sharp and blurred images in our work. The gradient of an image f can be calculated by the following formula:

$$g_x(i, j) = |f(i + 1, j) - f(i, j)| \tag{7}$$

$$g_y(i, j) = |f(i, j + 1) - f(i, j)| \tag{8}$$

where $g_x(i, j)$ and $g_y(i, j)$ are the gradients of the image f in the X and Y directions, respectively. According to the

image gradient, the fuzzy judgment evaluation coefficient calculation formula is:

$$FJC = \frac{1}{M \times N} \sum_{i=1}^{M} \sum_{j=1}^{N} \sqrt{\frac{(g_x(i,j))^2 + (g_y(i,j))^2}{2}} \times \frac{G_n}{512} \tag{9}$$

where G_n is the sum of the number of non-zero gradient values of the X-direction gradient map and the Y-direction gradient map. M, N are the number of rows and columns in the X and Y directions of the image, respectively. According to the experiment, the threshold T is selected. If FJC > T, it can be determined that the image is a clear image and no subsequent processing is needed. When FJC < T, the image can be considered as blurred, so that subsequent deblurring processing will be performed. In our experiments, T = 4, the choice of this threshold is related to the experimental environment, platform and test data.

2) MOTION BLURRED IMAGE DETERMINATION

Our system is designed to process motion blur images, so it is desirable to input blurred images that are missing information due to relative motion. It is also necessary to discriminate whether the blurred image is a motion blurred image before processing the blurred image. Since different types of blurred images undergo Fourier transform, the results vary greatly. Specifically, when the gradient image of the motion blurred image is converted into the frequency domain, a regular structure composed of parallel splines appears in the power spectrum in the frequency domain, and the other fuzzy images do not exhibit such a regular pattern. So we distinguish the blur type of the image according to the difference of the frequency spectrum in our work.

The gradient of the image f at a certain point (x, y) can be defined as a two-dimensional column vector, that is, the partial derivative of the point is obtained.

$$\nabla f = [G_x \ G_y]^T = \left[\frac{\partial f}{\partial x} \ \frac{\partial f}{\partial y}\right]^T \tag{10}$$

Usually the modulus of this vector is called the gradient, and the gradient can also be calculated by the following formula:

$$\nabla f = \sqrt{G_x^2 + G_y^2} = \sqrt{\left(\frac{\partial f}{\partial x}\right)^2 + \left(\frac{\partial f}{\partial y}\right)^2} \tag{11}$$

The discrete Fourier transform formula of the two-dimensional discrete function f(x, y) is as follows:

$$F(u,v) = \frac{1}{M \times N} \sum_{x=0}^{M-1} \sum_{y=0}^{N-1} f(x,y) e^{-j2\pi(\frac{ux}{M} + \frac{vy}{N})} \tag{12}$$

$F(u, v)$ is expressed in polar coordinates as:

$$F(u,v) = |F(u,v)| \, e^{j\theta(u,v)} = \sqrt{R^2(u,v) + I^2(u,v)} e^{j\theta(u,v)} \tag{13}$$

where $R(u, v)$ and $I(u, v)$ are the real and imaginary parts of $F(u, v)$, respectively, and $|F(u, v)|$ is the frequency spectrum of the Fourier transform, $\theta(u, v)$ is the phase angle. In order to judge the fuzzy image category more easily, the gradient image spectrum of the image is acquired by normalization. The normalized gradient spectrum T_d is calculated as follows:

$$T_d = \frac{tf - tf_{min}}{tf_{max} - tf_{min}} \tag{14}$$

where tf is the gradient image spectrum of the image, and tf_{min} and tf_{max} are the maximum and minimum values of the gradient image spectrum, respectively.

C. DESIGN OF MOBILE-DELUR SYSTEM

The blurred pictures can be viewed as a degraded images for a typical linear system. We have:

$$O(x,y) = F(x,y) * C(x,y) + s(n) \tag{15}$$

where O(x,y) represents the original blurred picture that the mobile device acquires. F(x,y) is point spread function, C(x,y) indicates a clear picture, s(n) represents additive noise, $*$ is a convolution operation. To deblur the image, we need to estimate the point spread function. In this work, we estimate the point spread function based on the motion of the camera. And we only consider the rotation of the 3D camera. On the one hand, the shutter speed of a smart phone is fast, and the blur of the photo is mainly caused by the rotation of the camera. On the other hand, camera panning requires the integration of two accelerometer data, with real-time drift, which is subject to errors.

Our idea is to use the gyroscope data from the phone to calculate the camera's orientation and then estimate the blur PSF. Since the output of the gyroscope is only suitable for orientation changes in short time intervals, and small errors will accumulate during the integration process, which results in gyro drift. In order to reduce the gyro drift, we use the method of [34], which combines the information of the accelerometer, magnetometer, and gyroscope to calculate the orientation of the 3D camera due to the magnetometer/accelerometer-based orientation provides long-term support information. The output of the method is the 3D camera orientation $\Theta(t) = (\theta_x(t), \theta_y(t), \theta_z(t))$ at time t.

1) SENSOR ASSISTED PSF ESTIMATION

In a pinhole camera, the image point x in homogeneous coordinates corresponds to the real-world three-dimensional coordinate point X:

$$x = CX \tag{16}$$

where C is the intrinsic camera matrix and c is given by:

$$C = \begin{pmatrix} f_x & 0 & w/2 \\ 0 & f_y & h/2 \\ 0 & 0 & 1 \end{pmatrix} \tag{17}$$

where w and h are the width and height of the image, respectively. f_x and f_y are unknown and are obtained by the calibration process. When the photo is captured during the exposure time of the camera, the position of the scene point

(x, y, z) on the image is $(u(t), v(t))$ at time t, which is the function of $p(t)$:

$$(u(t), v(t), 1)^T = P(t)(X, Y, Z, 1)^T \tag{18}$$

$P(t)$ changes over time, causing the fixed points in the scene to be projected to different positions at each moment. The projected trajectory of each point on the image plane is the PSF k of that point. We only need to know the relative motion of the camera during the exposure interval for image recovery, the plane homology method can be used to model this relative motion, which maps the initial projection of points at t_1 to another time t_2:

$$(u(t_2), v(t_2), 1)^T \simeq H(t_1, t_2)(u(t_1), v(t_1), 1)^T \tag{19}$$

$$H(t_1, t_2) = CR(t_2)R(t_1)^{-1}C^{-1} \tag{20}$$

We record two sets of orientation for each captured photo, $\Theta(t_1)$,$\Theta(t_2)$ are the camera orientation before and after the device captures the photo. And the corresponding camera rotation matrices $R(t_2)$ and $R(t_2)$ are calculated according to $\Theta(t_1)$ and $\Theta(t_2)$, respectively. According to equation (19), we can get a line between point $(u(t_1), v(t_1), 1)^T$ and point $(u(t_2), v(t_2), 1)^T$ with length $d(t_1, t_2)$. Then the spatial invariant k_r caused by camera rotation is modeled as 2D Gauss, and its center is $(u_k + \beta(u(t_2) - u(t_1)), v_k + \beta(v(t_2) - v(t_1)))$, the variances of the two axes are $\gamma d(t_1, t_2)$ and $\gamma d(t_1, t_2)/3$, respectively, (u_k, v_k) is the center of the kernel k. β and γ are scale factors and their values depend on the blur scale.

There is a fairly small time delay $\sigma(t)$ between the moment when the user presses the camera shutter and the actual time when the camera captures the photo. During this time, the camera's motion can be assumed to be constant, it mainly from the movement of the finger when the screen is pressed, and the effect of the motion is similar to the out-of-focus blur. Gaussian fuzzy kernel k_c can be used to model this blurring effect. The k_c center is located at (u_k, u_k) with variance $\delta = 2.0$ or 3.0 along both axes, respectively, for small and medium to large blur. Combining k_c and k_r, we can get psf k:

$$k = \alpha k_r + (1 - \alpha)k_c \tag{21}$$

where f_x, f_y and the correspondence of the sensor axes to the camera axes need to be determined, we use the method of [34], which uses a set of consecutive photos to verify our system. Assume that each photo has a small constant motion, the average orientation $(\Theta(t_1) + \Theta(t_2))/2$ before and after the capture is used as the orientation of the photo. Match points are detected from adjacent photos based on SURF features and RANSAC matching. The set of points matching $M = \{(u_i, u_i, v_j, v_j)\}$ can be used as ground truth to formulate an optimization problem for calibration:

$$\min_{f_x, f_y} \sum\nolimits_{i,j \in M} \left\| (u_i, v_i)^T - H(i, j)(u_j, v_j)^T \right\|^2 \tag{22}$$

2) NON-LINEAR DEBLURRING SYSTEM

The non-linear deblur system [3] consists of two parts. Np which estimates pixel region of the picture moving and Ep which estimates the edge pixel. Np is mainly used to calculate the degree of blur and determine how many pixel areas the target occupies in the image. Np is defined as:

$$N_p = \Sigma_{(x,y) \in O} QO(X, Y)[\frac{cos(vfT\pi)}{v\pi}]^{-1} exp(\frac{x^2 + y^2}{2\sigma_x \sigma_y}) + A \tag{23}$$

where $O(X, Y)$ represents each pixel of the original blurred image, Q is the blur level of the picture, and A is the intensity of the background.

The second part is the Ep that performs edge detection on the target in the image where the edge pixels whose background image and target image are unequal in color. Roberts operator searches for edge pixels by continuously calculating local pixel differentials, which is used to estimate Ep:

$$E_p = \{[\sqrt{O(x, y)} - \sqrt{O(x + 1, y + 1)}]^2 + [\sqrt{O(x + 1, y)} - \sqrt{O(x, y + 1)}^2]^2\}^{\frac{1}{2}} \tag{24}$$

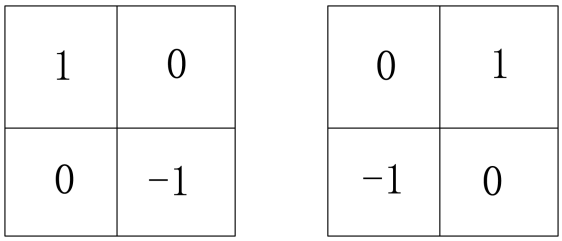

FIGURE 3. Detection operator template of Roberts.

The detection operator template is shown in Figure 3. Using two numbers of diagonal lines to convolution the pixel to get the (24). The non-linear deblurring system function $S(x, y)$ consists of N_p and E_p:

$$S(x, y) = N_p + E_p \tag{25}$$

The non-linear deblurring system takes the point spread function as a boundary limit, which is mapped to the blurred picture taken by mobile phone directly could do deblurring process.

3) WEINER-HOFF OPTIMIZATION

In order to achieve a better deblurring effect, we have optimized the system. First, the blurred image is denoised using median filtering. The basic idea of the algorithm is to replace the pixels of the blurred image with the intermediate points of the points in the neighborhood. The optimization of the median filter is defined as:

$$\widehat{O(x, y)} = Replace_{O(x,y) \in W}\{O(x, y)\} \tag{26}$$

O(x, y) is the pixel of the blurred picture, W is the denoising window, and Replace is the replacement algorithm. For each pixel value of a blurred picture, it is replaced with the intermediate value of each point in its neighborhood. The processed picture can be recorded as:

$$\overline{O(x, y)} = \Sigma^{+\infty}_{(x,y)=0} S(x, y)\widehat{O(x, y)} \tag{27}$$

(a) Original image. (b) Be noised image. (c) 7×7 Median filtering. (d) 9×9 Median filtering.

(e) 2D wiener-filtering. (f) Mean filtering. (g) Gaussian filtering. (h) P-M filtering.

FIGURE 4. Comparison of preprocessing results of different algorithms.

Mean square error J before and after image processing can be written as:

$$\begin{aligned} J &= [\{\overline{O(x,y)} - O(x,y)\}^2] \\ &= [\{\Sigma_{(x,y)=0}^{+\infty} S(x,y)\widehat{O(x,y)} - O(x,y)\}^2] \end{aligned} \tag{28}$$

Scan all the processed clear photos so that the average variance J of $\overline{O(x,y)}$ and the original blurred image O(x,y) satisfies the Wiener-Hoff equation, that is J satisfies the minimum value of the mean square error function, our system achieves optimal performance. The derivative of formula (28) is the following:

$$R(J) = 2\{\Sigma_{(x,y)=0}^{+\infty} S(x,y)\widehat{O(x,y)} - O(x,y)\} \tag{29}$$

The right side of formula (29) is the discrete equation of Wiener-Hoff. We set the discrete equation is zero:

$$\begin{aligned} R(J) &= 2\{\Sigma_{(x,y)=0}^{+\infty} S(x,y)\widehat{O(x,y)} - O(x,y)\} \\ &= 0 \end{aligned} \tag{30}$$

By considering the (23), (24), (25) and (30), the minimum mean square error J will satisfy:

$$J = \frac{(1-A)cos(vft\pi)}{Qv\pi} exp(\frac{2\sigma_x\sigma_y}{x^2+y^2}) \tag{31}$$

where Q is the equilibrium factor in this intensity of the background. V is horizontal relative velocity between the camera of mobile phone and target. The SID system will be globally optimized when the mean square error satisfies this condition.

V. IMPLEMENTATION AND EVALUATION

It is very important to preprocess the blurred image taken by the mobile phone. It can eliminate the hardware noise of the mobile phone sensor when taking pictures, and preserve the original picture features of the photo, thereby improving the performance of the SID system. We first do a benchmark experiment to verify the performance of our P-M nonlinear diffusion model for preprocessing the image.

A. PERFORMANCE OF P-M NONLINEAR DIFFUSION MODEL

In order to verify the validity of the p-m nonlinear diffusion model, we use median filtering, Gaussian filtering, wavelet denoising and p-m nonlinear diffusion model to preprocess the original image with hardware noise. Figure 4 shows the results of their processing. The comparison between the above pictures shows that 2D Wiener filtering and Mean filtering are not effective, the Gaussian denoising and blurring edge, while the P-M model can not only remove the noise but also retain the edge and texture details well. So the pretreatment effect of the p-m nonlinear diffusion model is very good.

B. PERFORMANCE OF BLURRED IMAGE DETERMINATION ALGORITHM

Before deblurring the image, we need to judge whether the input image is fuzzy and whether it is a motion blur picture, which not only improves the efficiency of the system,

(a) Original blurred stationary picture due to the hand slight jitter.

(b) Processed image.

(c) Original blurred picture because the car moves quickly.

(d) Processed image.

(e) Original blurred picture caused by virtual focus.

(f) Processed image.

(g) Original blurred picture caused by light.

(h) Processed image.

FIGURE 5. Comparison of different blurred pictures before and after system processing.

TABLE 1. Image recognition result.

Image category	Clear image	Blurred image	Motion blurred image	Accuracy
Clear image	91	5	0	91%
Blurred image	9	87	16	87%
Motion blurred image	0	8	84	84%

but also avoids damage to the original high quality image. In the experiment, we tested the performance of our image deblurring judgment algorithm with 300 pictures of different blur categories, and the blurred image refers to other types of blurred images that do not include a motion blurred image. Image recognition results are shown in the table 1, the recognition accuracy of the blurred image is 87%, and the correct recognition accuracy of the motion blurred image is 84%, indicating that our image determination algorithm can correctly identify blurred images in most cases.

C. PERFORMANCE OF WEINER-HOFF OPTIMIZATION

In order to achieve better deblurring effect, we designed a Wiener-Hoff optimization module to optimize the output image of the nonlinear deblurring system. In the experiment, we analyzed the gray levels before and after the optimization of 400 different fuzzy images. The experimental results are shown in FIGURE 6. The green line indicates the gray distribution of the image before optimization, and the red line indicates the gray distribution of the optimized image. It can be seen that the optimized image gray distribution is more stable and uniform, indicating that the image is more clear after optimization, because the higher the sharpness, the more uniform the gray distribution, and the image pixels occupy more possible gray levels.

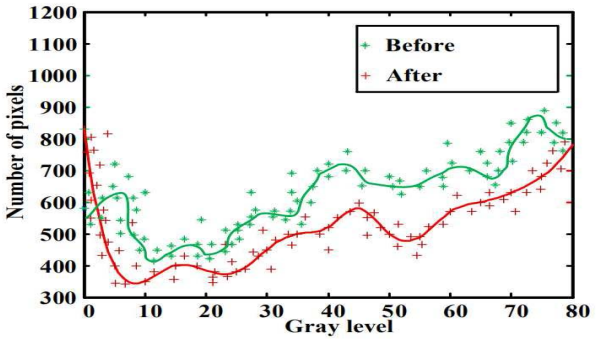

FIGURE 6. Gray-scale distribution before and after deblurred image optimization.

D. PERFORMANCE OF SID IN DIFFERENT SCENARIOS

We deployed our system experiments on Android phones. We take pictures of the target of interest in the still and moving

scenes respectively, and then preprocess the image with the P-M pre-processing model. The pre-processed photos are then deblurred by the SID system.

In the experiment, we first select a cup on the table as the target object, let the user capture the target during the walking process, which is equivalent to deploy an experimental scene with micro-vibration of the arm. In this process, the micro-vibration of the arm will inevitably lead to the camera unstable. The captured photos are blurred at different levels depending on the level of hand shaking. Figure 5(a) shows the blurred image caused by the micro-jitter of the arm during the walking process. The image restoration effect after deblurring by our SID system is shown in Figure 5(b). It can be seen from the visual effect that the contour of the cup is blurred due to the vibration of the user's arm, and the processed picture becomes more clear.

When the user captures a fast moving target of interest, a blurred image with a more severe degree of jitter is captured, as shown in Figure 5(c), and the image processed by the system is as shown in Figure 5(d). Obviously, the image after processing has a better visual effect, indicating that our system has a good performance. In addition, for low-quality images of non-motion blur types (such as blurred images caused by virtual focus and lighting problems), we have also experimented accordingly. The images before and after the SID system processing are shown in Figure 5(e) to Figure 5(h), and the image after processing is much clearer than before. A group simple experiment in four different scenarios verifies that the SID system has a significant deblurring effect from a visual perspective.

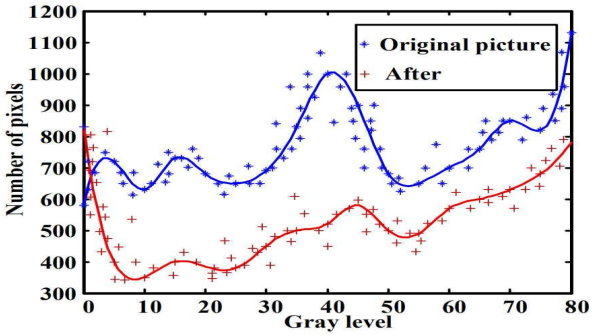

(a) The gray level before and after image processing in a slight vibration scene.

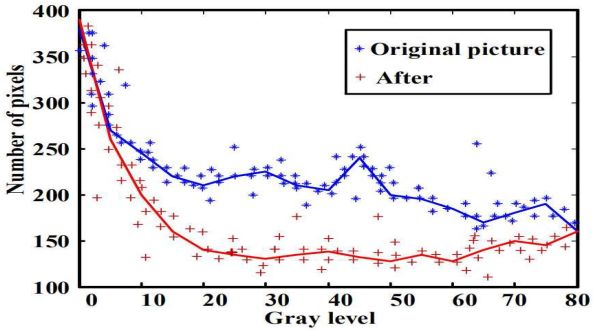

(b) the gray level comparison before and after image processing in a strong vibration scene.

FIGURE 7. Comparison of gray levels before and after image processing in different vibration scenes.

E. SYSTEM PERFORMANCE INDICATORS

Common indicators of image clarity include image grayscale, light distribution, spectrum, etc. In order to better verify the image recovery performance of SID system, we analyze the related indexes before and after image processing in different experimental scenes.

1) GRAY LEVEL OF THE IMAGE

The sharper the image, the more uniform and stable the gray scale distribution, since the image pixels occupy all possible gray levels. Figure 7(a) shows the gray level distribution curve before and after the slight blurred image processing. It can be seen that the gray scale distribution of the image after processing by the system is more stable. The image has high contrast and variable gray tone, and more clearer. Figure 7(b) shows the gray distribution curve before and after the image processing with high ambiguity captured by the user in a fast moving scene. It can be seen that the gray distribution of the processed image is more stable, indicating that the processed image quality is higher than before. Which also reflects the effectiveness of the deblurring system.

2) THE LIGHT DISTRIBUTION OF THE IMAGE

For fuzzy pictures, the light distribution is relatively uniform and the parameter curve is relatively stable. With the processed image, the target contour has a sharpening effect, and the light distribution has obvious peaks at the edge of the target contour. The results of the light distribution before and after the image processing of the above two different degrees of blur are as shown in Figure 8(a) and Figure 8(b), in which there is a portion where the light is coincident before and after the processing, and by the search of the pixel points, the coincident portion is the picture. The background light is not the main target of the picture, and the bright curve has obvious changes at the edge of the target contour, which should be presented after the picture is sharpened. It is confirmed once again that the SID system has certain feasibility and superiority in the image deblurring problem.

3) SPECTRAL ANALYSIS OF IMAGES

The clearer the picture, the more detailed information it contains, and the more high frequency components it contains in the spectrogram. Therefore, in order to detect the deblurring effect of the system, We do spectrum analysis [20] for pictures before and after processing in different experimental scenarios, and the results are shown in the Figure 9. It can be seen that the white point with the high frequency component as the center point in Figure 9(a) covers a small range, while the white point coverage in 9(b) is wider, indicating that the detailed information content of the image after processing is more than the before. The picture is clearer before processing.

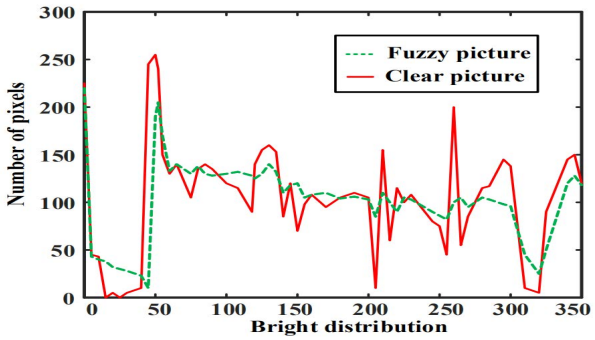

(a) Brightness distribution before and after image processing in a slight vibration scene.

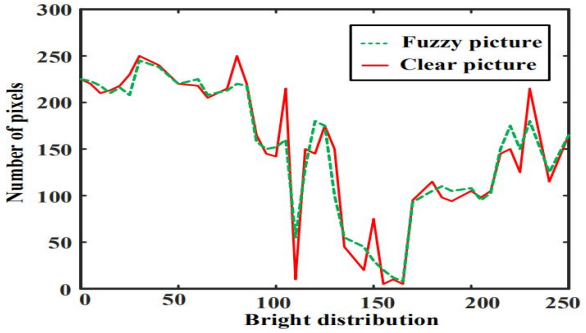

(b) Brightness distribution before and after image processing in a strong vibration scene.

FIGURE 8. Comparison of brightness distribution before and after image processing in different vibration scenes.

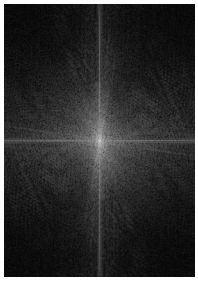

(a) Spectrum of the original picture in a slight vibration scene.

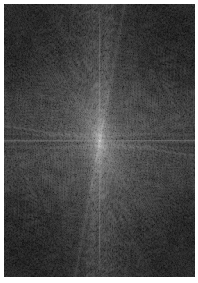

(b) After process.

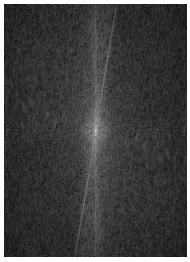

(c) Spectrum of the original picture in a strong vibration scene.

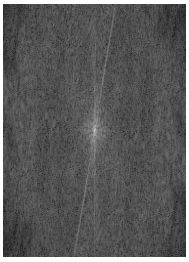

(d) After process.

FIGURE 9. Spectrogram before and after image processing in different vibration scenarios.

Figure 9(c) and 9(d) show the spectrum analysis of the picture in the second scenario. Through the comparison of the spectrograms, it is also well illustrated that the deblurring system of the mobile terminal can improve the quality of the blurred picture very well.

4) SYSTEM PROCESSING DELAY

Our deblurring system is implemented on mobile terminals, and the computational delay must also be taken care of. Compared with the traditional mobile phone to obtain pictures and then use a dedicated image processor to complete the deblurring process, the system has a certain timeliness and convenience. We deployed experiments on Android smart phones, and processed 100 images of different sizes and different degrees of blur in the four scenarios, and analyzed the delay. The overall latency of the SID system averaged 6 to 7 seconds. Figure 10(a) shows the distribution of image processing delays at different degrees of blur. The yellow dotted line indicates the delay curve of the severely dithered picture, and the red line indicates the fuzzy picture processing delay distribution of the micro-vibration. It can be seen that the performance of the SID system is relatively consistent regardless of the slightly blurred picture or the severely blurred picture, and the SID delay performance does not change significantly with the size of the picture, and has strong robustness.

We also compare the processing delays of traditional methods. The most commonly used blind recovery algorithms typically require 5 to 12 times of iterative calculations to calculate the point spread function, with an average processing delay of between 9 and 10 seconds. Figure 10 shows the average delay distribution for traditional methods and SID systems. Processing latency of the SID system is reduced by approximately 3 seconds, and the latency performance does not vary significantly depending on the picture size. Compared to traditional methods, SID systems have less processing delay and are more suitable for mobile devices.

VI. RELATED WORK

A. TRADITIONAL IMAGE DEBLURRING METHODS

Image deblurring is a process of deconvolution. The RL deconvolution restoration algorithm [22] which assumes that the blurred image is an iterative algorithm affected by poisson distribution. It obtains the most likely estimate of the clear image by the maximum likelihood method. However, the RL algorithm has the disadvantages of noise amplification and ringing effects. In response to the shortcomings of this algorithm, Lagendijk *et al.* [16] proposed a residual deconvolution method, which reduces the ringing effect, But the deblurring effect is not ideal when the noise is very large.

The inverse filtering method proposed by Tugnait [32], which is the first image restoration algorithm to convert a blurred image from a spatial domain to a frequency domain. The algorithm is simple and the computational overhead is small. But the noise and ringing effects are still large, and the point spread function [29] is usually unknown, these shortcomings limit the use of the inverse filtering method on mobile devices. Due to the ringing effect of inverse filtering algorithm on image restoration, Wang *et al.* proposed

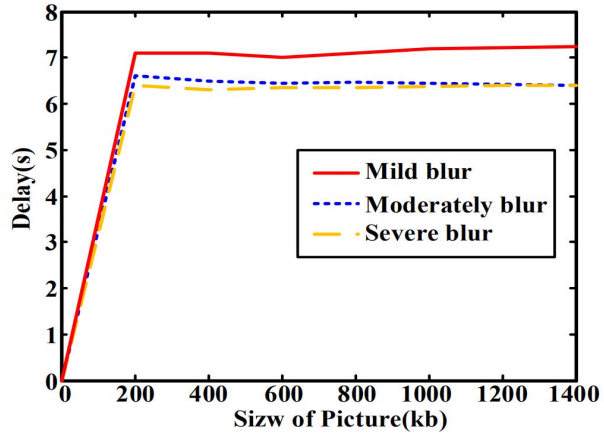

(a) Delay of micro, moderate and strong vibration scenes.

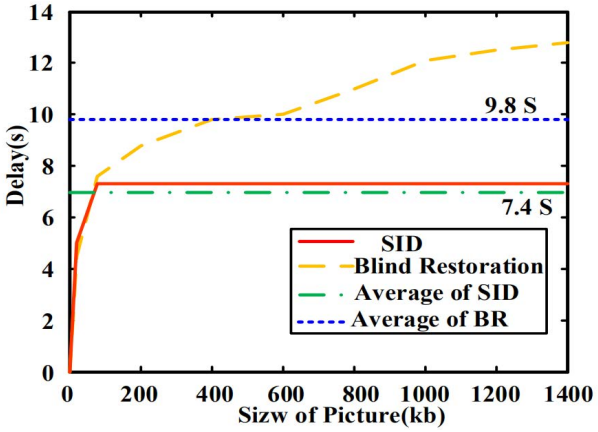

(b) Comparison of processing delays for different methods.

FIGURE 10. **The processing delay of the pictures in different scenes.**

an image smoothing method [33], which use neighborhood mean method and the weighted average method to smooth spatial images to reduce the image noise. Wiener filtering [13] is a linear filter with the minimum mean square error as the optimal criterion, the image restoration effect is ideal when the frequency properties and noise of the image are known. Yang *et al.* used a two-dimensional Wiener filtering method [38] which make full use of images and their noise information. The performance is better when the image is affected by noise. These methods are either too computationally intensive or rely on other information to obtain a point spread function and cannot be used on mobile devices with limited resources.

B. IMAGE DEBLURRING METHODS BASED ON INERTIAL SENSOR MEASUREMENTS

Previous studies have shown that blurred images can be represented as integrals of all intermediate images captured by the camera along motion trajectories [37], [42]. The motion of the camera can be modeled as in-plane translation and rotation [10]. Reference [30] proposed an intelligent deblurring system based on gyro reading synthesis of local fuzzy kernel. Compared with the existing deblurring algorithm, the system has a good effect, but requires manual synchronization of the camera and the gyro sensor. Josh *et al.* [14] established a well-designed DSLR-based camera system, assuming that the inertial sensors are pre-calibrated and synchronized. However, due to drift problems with noise sensor reading, efficient image deblurring cannot be performed using a single sensor data.

Some works correct image sensor parameters using image priority or multiple images [14], [23]. Most of the work assumes that the sensor data they record is reliable, or that this assumption is only slightly relaxed. However, smart phone inertial sensors do not provide high quality data for efficient image deblurring. Instead, our approach does not estimate the motion of the camera directly from a single sensor, as done in these previous techniques [14], [30]. We use the orientation of the magnetometer/accelerometer as the long-term support information, the output of the gyroscope is only used for the orientation change of short time interval, and we use a set of consecutive photos to calibrate our system, the calibration process for each device is only required to be performed once.

VII. CONCLUSION

We proposed a sensor-assisted image deblurring system for mobile devices targeting at photos captured by hand-held smart phones. The camera motion information is obtained by fusing the output of the built-in sensor of the smart phone, and then estimating the PSF. The P-M nonlinear extended model removes the noise while retaining the image information well. The fuzzy image confirmation avoids the damage to the original clear image. The nonlinear deblurring improves the linear sensitivity of the system. Wiener Hoff optimization optimized the deblurring performance of the system. Experiments on Android mobile devices have shown that our approach is more efficient and robust than traditional algorithms in the prior art.

REFERENCES

[1] S. K. Nayar and M. Ben-Ezra, "Motion-based motion deblurring," *IEEE Trans. Pattern Anal. Mach. Intell.*, vol. 26, no. 6, pp. 689–698, Jun. 2004.
[2] J. Besag, J. York, and A. Mollié, "Bayesian image restoration, with two applications in spatial statistics," *Ann. Inst. Stat. Math.*, vol. 43, no. 1, pp. 1–20, Mar. 1991.
[3] B. Bilgehan, "Efficient approximation for linear and non-linear signal representation," *IET Signal Process.*, vol. 9, no. 3, pp. 260–266, Apr. 2015.
[4] S. Chang, H. Zhu, W. Zhang, L. Lu, and Y. Zhu, "PURE: Blind regression modeling for low quality data with participatory sensing," *IEEE Trans. Parallel Distrib. Syst.*, vol. 27, no. 4, pp. 1199–1211, Apr. 2016.
[5] L. Fedeli, I. Gerace, and F. Martinelli, "Unsupervised blind separation and debluring of mixtures of sources," in *Proc. Int. Conf. Knowl.-Based Intell. Inf. Eng. Syst.*, 2007, pp. 25–32.
[6] R. Fergus, B. Singh, A. Hertzmann, S. T. Roweis, and W. T. Freeman, "Removing camera shake from a single photograph," *ACM Trans. Graph.*, vol. 25, no. 3, pp. 787–794, 2006.
[7] H. Gao, W. Huang, Y. Duan, X. Yang, and Q. Zou, "Research on cost-driven services composition in an uncertain environment," *J. Internet Technol.*, vol. 20, no. 3, pp. 755–769, 2019.
[8] H. Gao, W. Huang, and X. Yang, "Applying probabilistic model checking to path planning in an intelligent transportation system using mobility trajectories and their statistical data," *Intell. Automat. Soft Comput.*, vol. 25, pp. 547–559, 2019.

[9] H. Gao, W. Huang, X. Yang, Y. Duan, and Y. Yin, "Towards service selection for workflow reconfiguration: An interface-based computing," *Future Gener. Comput. Syst.*, vol. 87, pp. 298–311, Oct. 2018.
[10] A. Gupta, N. Joshi, C. L. Zitnick, M. Cohen, and B. Curless, "Single image deblurring using motion density functions," in *Proc. Eur. Conf. Comput. Vis.*, 2010, pp. 171–184.
[11] M. Hirsch, C. J. Schuler, S. Harmeling, and B. Schölkopf, "Fast removal of non-uniform camera shake," in *Proc. IEEE Int. Conf. Comput. Vis.*, Nov. 2011, pp. 463–470.
[12] P. Hu, H. Ning, T. Qiu, Y. Xu, X. Luo, and A. K. Sangaiah, "A unified face identification and resolution scheme using cloud computing in Internet of Things," *Future Gener. Comput. Syst.*, vol. 81, pp. 582–592, Apr. 2017.
[13] J. Chen, J. Benesty, Y. Huang, and S. Doclo, "New insights into the noise reduction Wiener filter," *IEEE Trans. Audio, Speech, Language Process.*, vol. 14, no. 4, pp. 1218–1234, Jul. 2006.
[14] N. Joshi, S. B. Kang, C. L. Zitnick, and R. Szeliski, "Image deblurring using inertial measurement sensors," *ACM Trans. Graph.*, vol. 29, no. 4, p. 30, Jul. 2010.
[15] R. Kohler, M. Hirsch, B. Mohler, B. Scholkopf, and S. Harmeling, *Recording and Playback of Camera Shake: Benchmarking Blind Deconvolution with a Real-World Database*. 2012.
[16] R. L. Lagendijk, J. Biemond, and D. E. Boekee, "Identification and restoration of noisy blurred images using the expectation-maximization algorithm," *IEEE Trans. Acoust., Speech, Signal Process.*, vol. 38, no. 31, pp. 1180–1191, Jul. 1990.
[17] N. D. Lane, S. Bhattacharya, P. Georgiev, C. Forlivesi, and F. Kawsar, "DeepX: A software accelerator for low-power deep learning inference on mobile devices," in *Proc. Int. Conf. Inf. Process. Sensor Netw. (IPSN)*, Apr. 2016, pp. 1–12.
[18] M. Ledoux, "Heat flow derivatives and minimum mean-square error in Gaussian noise," *IEEE Trans. Inf. Theory*, vol. 62, no. 6, pp. 3401–3409, Jun. 2016.
[19] F. Lindgren, H. Rue, and J. Lindstrom, "An explicit link between Gaussian fields and Gaussian Markov random fields: The stochastic partial differential equation approach," *J. Roy. Stat. Soc.*, vol. 73, no. 4, pp. 423–498, 2011.
[20] A. Liutkus and R. Badeau, "Generalized wiener filtering with fractional power spectrograms," in *Proc. IEEE Int. Conf. Acoust., Speech Signal Process. (ICASSP)*, Apr. 2015, pp. 266–270.
[21] R. Lun, C. Gordon, and W. Zhao, "Tracking the activities of daily lives: An integrated approach," in *Proc. Future Technol. Conf. (FTC)*, Dec. 2017, pp. 466–475.
[22] N. Milad, R. Hossein, and B. Z. Massoud, "Image restoration using Gaussian mixture models with spatially constrained patch clustering," *IEEE Trans. Image Process.*, vol. 24, no. 11, pp. 3624–3636, Nov. 2015.
[23] S. H. Park and M. Levoy, "Gyro-based multi-image deconvolution for removing handshake blur," in *Proc. IEEE Conf. Comput. Vis. Pattern Recognit.*, Jun. 2014, pp. 3366–3373.
[24] L. Qi, S. Meng, X. Zhang, R. Wang, X. Xu, Z. Zhou, and W. Dou, "An exception handling approach for privacy-preserving service recommendation failure in a cloud environment," *Sensors*, vol. 18, no. 7, p. 2037, 2018.
[25] L. Qi, R. Wang, S. Li, Q. He, X. Xu, and C. Hu, "Time-aware distributed service recommendation with privacy-preservation," *Inf. Sci.*, vol. 480, pp. 354–364, Apr. 2019.
[26] L. Qi, X. Xu, W. Dou, J. Yu, Z. Zhou, and X. Zhang, "Time-aware IoE service recommendation on sparse data, mobile information systems," *IEEE J. Sel. Areas Commun.*, to be published.
[27] L. Qi, X. Zhang, W. Dou, C. Hu, C. Yang, and J. Chen, "A two-stage locality-sensitive hashing based approach for privacy-preserving mobile service recommendation in cross-platform edge environment," *Future Gener. Comput. Syst.*, vol. 88, pp. 636–643, Nov. 2018.
[28] L. Qi, X. Zhang, W. Dou, and Q. Ni, "A distributed locality-sensitive hashing-based approach for cloud service recommendation from multi-source data," *IEEE J. Sel. Areas Commun.*, vol. 35, no. 11, pp. 2616–2624, Nov. 2017.
[29] F. Santi, M. Antoniou, and D. Pastina, "Point spread function analysis for GNSS-based multistatic SAR," *IEEE Geosci. Remote Sens. Lett.*, vol. 12, no. 2, pp. 304–308, Feb. 2015.
[30] O. Sindelar and F. Sroubek, "Image deblurring in smartphone devices using built-in inertial measurement sensors," *J. Electron. Imag.*, vol. 22, no. 1, Feb. 2013, Art. no. 011003.
[31] T. Song, S. Pang, S. Hao, A. Rodrguez-Paton, and P. Zheng, "A parallel image skeletonizing method using spiking neural P systems with weights," *Neural Process. Lett.*, vol. 3, pp. 1–18, Oct. 2018.
[32] J. K. Tugnait, "Identification and deconvolution of multichannel linear non-Gaussian processes using higher order statistics and inverse filter criteria," *IEEE Trans. Signal Process.*, vol. 45, no. 3, pp. 658–672, Mar. 1997.
[33] Y. Wang, Q.-F. Zhu, and L. Shaw, "Maximally smooth image recovery in transform coding," *IEEE Trans. Commun.*, vol. 41, no. 10, pp. 1544–1551, Oct. 1993.
[34] J. Wei, D. Zhang, and H. Yu, "Sensor-assisted image deblurring of consumer photos on smartphones," in *Proc. IEEE Int. Conf. Multimedia Expo (ICME)*, Jul. 2014, pp. 1–6.
[35] W. Xi, J. Zhao, X.-Y. Li, K. Zhao, S. Tang, X. Liu, and Z. Jiang, "Electronic frog eye: Counting crowd using WiFi," in *Proc. IEEE Conf. Comput. Commun.*, Apr./May 2015, pp. 361–369.
[36] Y. Weng, T. Zhou, L. Liu, and C. Xia, "Automatic convolutional neural architecture search for image classification under different scenes," *IEEE Access*, vol. 7, pp. 38495–38506, 2019.
[37] O. Whyte, J. Sivic, A. Zisserman, and J. Ponce, "Non-uniform deblurring for shaken images," in *Proc. IEEE Comput. Soc. Conf. Comput. Vis. Pattern Recognit.*, Jun. 2010, pp. 491–498.
[38] L. Yang, Y. Li, Q. Lin, X. Y. Li, and Y. Liu, "Making sense of mechanical vibration period with sub-millisecond accuracy using backscatter signals," in *Proc. Int. Conf. Mobile Comput. Netw.*, Oct. 2016, pp. 16–28.
[39] X. Yin, W. Shen, and X. Wang, "Incremental clustering for human activity detection based on phone sensor data," in *Proc. IEEE 20th Int. Conf. Comput. Supported Cooperat. Work Design (CSCWD)*, May 2016, pp. 35–40.
[40] Y. Yin, S. Aihua, G. Min, X. Yueshen, and W. Shuoping, "QoS prediction for Web service recommendation with network location-aware neighbor selection," *Int. J. Softw. Eng. Knowl. Eng.*, vol. 26, no. 4, pp. 611–632, 2016.
[41] Y. Yin, F. Yu, Y. Xu, L. Yu, and J. Mu, "Network location-aware service recommendation with random walk in cyber-physical systems," *Sensors*, vol. 17, no. 9, p. 2059, 2017.
[42] Y.-W. Tai, P. Tan, and M. S. Brown, "Richardson-lucy deblurring for scenes under a projective motion path," *IEEE Trans. Pattern Anal. Mach. Intell.*, vol. 33, no. 8, pp. 1603–1618, Aug. 2011.
[43] J. Zhao, W. Xi, Y. He, Y. Liu, X.-Y. Li, L. Mo, and Z. Yang, "Localization of wireless sensor networks in the wild: Pursuit of ranging quality," *IEEE/ACM Trans. Netw.*, vol. 21, no. 1, pp. 311–323, Feb. 2013.

QING WANG received the B.S. degree in computer science from Northwest University, Xi'an, China, in 2017, where she is currently pursuing the master's degree. Her main research interests include wireless signal processing and mobile computing.

JUN TAN received the B.S. degree in computer science from Northwest University, Xi'an, China, in 2016, where she is currently pursuing the master's degree. Her main research interests include mobile equipment and wearable technology.

TIANZHANG XING received the B.E. degree from the School of Communications Engineering, Xidian University, in 2004, and the Ph.D. degree in computer science from Northwest University, Xi'an, China, in 2015, where he is currently an Associate Professor with the School of Information Science and Technology. His current research interest includes wireless communication networks, with emphasis on the localization problem and mobile computing.

FENG CHEN received the Ph.D. degree in computer science and technology from Northwestern Polytechnical University, Xi'an, China, in 2012. His current research interests include localization and performance issues in wireless ad hoc, mesh, and sensor networks.

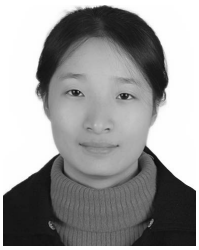

JINPING NIU received the Ph.D. degree from Xidian University, Xi'an, China, in 2014. She was a Visiting Student with the School of Electrical and Computer Engineering, Georgia Institute of Technology, Atlanta, GA, USA, from 2011 to 2013. She is currently a Lecturer with the School of Information Science and Technology, Northwest University, Xi'an. Her research interests include signal processing and resource allocation for wireless communication systems.